Mon. Not. R. Astron. Soc. **381,** 367–376 (2007) doi:10.1111/j.1365-2966.2007.12279.x

Dependence of the local reionization history on halo mass and environment: did Virgo reionize the Local Group?

Simone M. Weinmann,[1⋆] Andrea V. Macciò,[1,2] Ilian T. Iliev,[3] Garrelt Mellema[4] and Ben Moore[1]

[1]*Institute for Theoretical Physics, University of Zurich, CH-8057 Zurich, Switzerland*
[2]*Max-Planck-Institute for Astronomy, Königstuhl 17, D-69117 Heidelberg, Germany*
[3]*Canadian Institute for Theoretical Astrophysics, University of Toronto, 60 St George Street, Toronto, ON, Canada M5S 3H8*
[4]*Stockholm Observatory, AlbaNova University Centre, Stockholm University, SE-106 91 Stockholm, Sweden*

Accepted 2007 July 26. Received 2007 July 25; in original form 2007 May 7

ABSTRACT

The reionization of the Universe has profound effects on the way galaxies form and on their observed properties at later times. Of particular importance is the relative timing of the reionization history of a region and its halo assembly history, which can affect the nature of the first stars formed in that region, the properties and radial distribution of its stellar halo, globular cluster population and its satellite galaxies. We distinguish two basic cases for the reionization of a halo – internal reionization, whereby the stars forming *in situ* reionize their host galaxy, and external reionization, whereby the progenitor of a galaxy is reionized by external radiation before its own stars are able to form in sufficient numbers. We use a set of large-scale radiative transfer and structure formation simulations, based on cosmologies derived from both *Wilkinson Microwave Anisotropy Probe* (*WMAP*) one-year and *WMAP* three-year data, to evaluate the mean reionization redshifts and the probability of internal/external reionization for Local Group-like systems, galaxies in the field and central cD galaxies in clusters. We find that these probabilities are strongly dependent on the underlying cosmology and the efficiency of photon production, but also on the halo mass. There is a rapid transition between predominantly external and predominantly internal reionization at a mass scale of $\sim 10^{12}$ $M_{\odot}$ (corresponding roughly to L^{*} galaxies), with haloes less massive than this being reionized preferentially from distant sources. We provide a fit for the reionization redshift as a function of halo mass, which could be helpful to parametrize reionization in semi-analytical models of galaxy formation on cosmological scales. We find no statistical correlation between the reionization history of field galaxies and their environment.

Key words: radiative transfer – galaxies: evolution – cosmology: theory – large-scale structure of Universe.

1 INTRODUCTION

The lack of Gunn–Peterson troughs in the spectra of distant galaxies and QSOs show that the Universe has been almost completely ionized ever since redshift $z \sim 6$. This reionization was a consequence of the ionizing radiation emitted by the first galaxies, which started forming at $z > 20$ through the gravitational growth of the primordial density fluctuations. The recent three-year results from the *Wilkinson Microwave Anisotropy Probe* (*WMAP*) satellite (Spergel et al. 2007) indicated that reionization was well advanced by $z \sim 10$ and was thus fairly extended in time. Reionization had some profound implications on star and galaxy formation. First, stars forming in a reionized medium of low metallicity are probably considerably less massive than stars forming in a neutral medium of low metallicity (e.g. Johnson & Bromm 2006) and follow a different evolutionary path. Secondly, the formation of low-mass galaxies is suppressed in the presence of an ionizing background. The shallow gravitational wells of the small haloes cannot hold on to their gas if the halo virial temperature is below $T_{\rm vir} \sim 10^4$ K (Dekel & Silk 1986; Shapiro, Iliev & Raga 2004; Iliev, Shapiro & Raga 2005), while for larger haloes (10^4 K $\lesssim T_{\rm vir} \lesssim 10^5$ K) the gas accretion rate decreases, and the cooling time of the gas increases, thereby suppressing further star formation (Efstathiou 1992; Thoul & Weinberg 1996; Navarro & Steinmetz 1997; Bullock, Kravtsov & Weinberg 2000; Dijkstra et al. 2004). Therefore, reionization is a promising candidate for

⋆E-mail: weinmann@physik.uzh.ch

reconciling the discrepancy between the number of observed low-luminosity satellite galaxies around the Local Group (LG) and the cold dark matter (CDM) simulation predictions, often referred to as the 'missing satellite problem' (Klypin et al. 1999; Moore et al. 1999; Tully et al. 2002). Thirdly, reionization may have truncated the formation of the blue, old globular clusters that are still observed today (Santos 2003; Moore et al. 2006). Since massive galaxies will be reionized considerably before reionization is completed in the entire intergalactic medium (IGM), it is interesting to ask when and how a galaxy of a given mass, located in a given environment, will be reionized.

Generically, there are two ways in which a galaxy can be reionized. The process could be driven by the radiation emanating from its own stars forming *in situ* ('internal reionization') or the galaxy or its progenitors could be overrun by the global ionization fronts created by objects which collapsed earlier ('external reionization'). The second scenario is expected to occur, e.g. for low-mass satellites that have been close to large galaxies like the Milky Way since before reionization, while the first scenario should be typical for very massive galaxies in the central regions of clusters. It is less clear what scenario should be expected for intermediate-mass galaxies. For example, a field galaxy which resides close to a massive cluster could have been reionized by the radiation coming from the protocluster before the galaxy itself formed. The concept of a non-uniform, density-dependent reionization redshift has been introduced by Barkana & Loeb (2004). They point out that external reionization may become important in underdense regions and voids, thus causing the relatively small number of dwarf galaxies in these regions.

In this work we study the reionization history of haloes and its dependence on the halo mass and environment. To this end, we explore data from series of large-scale structure formation and radiative transfer (RT) simulations of cosmic reionization. We resimulate the same initial conditions at lower resolution which allows for tagging of the particles and thus for following the detailed merger and accretion history of haloes from the reionization epoch to the present. This allows us to identify the progenitors of massive cluster galaxies, field galaxies and LG-like systems and simultaneously follow both their reionization history and their mass growth history.

In this paper, we will use two different flat ΛCDM cosmologies, the first with parameters $(\Omega_\mathrm{m}, \Omega_\Lambda, \Omega_\mathrm{b}, h, \sigma_8, n) = (0.27, 0.73, 0.044, 0.7, 0.9, 1)$ (Spergel et al. 2003, hereafter *WMAP*1) and $(\Omega_\mathrm{m}, \Omega_\Lambda, \Omega_\mathrm{b}, h, \sigma_8, n) = (0.24, 0.76, 0.042, 0.73, 0.74, 0.95)$ (Spergel et al. 2007, hereafter *WMAP*3). Here Ω_m, Ω_Λ and Ω_b are the total matter, vacuum and baryonic densities in units of the critical density, h is the Hubble constant in units of 100 km s^{-1} Mpc^{-1}, σ_8 is the standard deviation of linear density fluctuations at present on the scale of $8\,h^{-1}$ Mpc and n is the index of the primordial power spectrum.

This paper is organized as follows. In Section 2 we summarize our simulations. In Section 3 we present our techniques used to select field haloes and follow the reionization histories of individual haloes. In Section 4 we present our results for the reionization histories of field galaxies, cD galaxies in the centres of galaxy clusters and LG-like objects. In Sections 5 and 6 we discuss potential caveats and discuss the implications of external versus internal reionization on the observable galaxy characteristics. Finally, in Section 7, we give a summary of our results.

2 SIMULATIONS

Our simulations follow the evolution of a comoving simulation volume of $(100\,h^{-1}\,\mathrm{Mpc})^3$. Our basic methodology and simulation parameters are described in detail in Iliev et al. (2006b), Mellema et al. (2006b), Iliev et al. (2007). Here we provide just a brief summary, in addition to a detailed discussion of the elements which are first presented in this work. See Table 1 for listing of the codes used in this work and their effective mass and spatial resolutions.

Table 1. Overview of the three different codes and the resolutions used in our *WMAP*3 simulation (*WMAP*1 is similar). Note that the spatial resolution in PMFAST is better by at least an order of magnitude as far as the positions of halo centres are concerned. In the PKDGRAV simulation, the spatial resolution is not clearly defined and was assumed to be equal to the force resolution.

	Code	Mass resolution ($h^{-1}\,\mathrm{M}_\odot$)	Spatial resolution
HR	PMFAST	2×10^7	$\sim 30\,h^{-1}$ kpc
LR	PKDGRAV	9.96×10^8	$\sim 10\,h^{-1}$ kpc
RT	C^2-RAY	–	$\sim 0.5\,h^{-1}$ Mpc

Table 2. Summary of the results. Listed are the mean redshift of formation, z_f, the mean starting redshift of the halo reionization, z_r, and the mean redshift at which 70 per cent of the final halo mass is reionized, $z_{70\,\mathrm{percent}}$, the fraction of objects reionized externally, f_ext, the average time interval between formation and reionization, $\Delta t \equiv t_\mathrm{f} - t_\mathrm{r}$ (in Myr), and Δt^*, which is the same time difference in units of the Hubble time when 50 per cent of the mass in the universe is ionized, for all of our simulations, as labelled. If Δt is negative, haloes are on average reionized *before* formation.

	z_f	z_r	$z_{70\,\mathrm{percent}}$	f_ext	Δt	Δt^*
*WMAP*1-f2000						
Field haloes	10.8	13.4	13.1	0.79	−114	−0.237
L* halo sample	12.6	13.6	12.85	0.62	−36	−0.075
Central cDs	16.7	15.5	14.1	0.0	26	0.055
LG sample	12.8	13.3	12.9	0.44	−21	−0.044
*WMAP*1-f250C						
Field haloes	11.0	11.7	10.4	0.4	−33	−0.053
L* halo sample	12.6	12.4	10.9	0.17	8	0.013
Central cDs	16.7	15.5	11.8	0.0	26	0.042
LG sample	12.8	12.4	10.8	0.1	13	0.021
*WMAP*3-f250C						
Field haloes	8.2	8.9	8.2	0.56	−60	−0.062
L* halo sample	9.3	9.4	8.6	0.27	−9	−0.009
Central cDs	13.0	12.6	9.6	0.0	15	0.016
LG sample	9.1	9.2	8.3	0.24	−8	−0.008

Table 3. Fitting parameters for $\langle z_\mathrm{r} \rangle\,(M)$, with $\langle z_\mathrm{r} \rangle = ax + bx^2 + cx^3$, where $x = \log(M/\mathrm{M}_\odot)$.

	a	b	c
*WMAP*1-f2000	5.079	−0.599	0.022
*WMAP*3-f250C	0.187	0.079	−0.001
*WMAP*3-f250C	1.592	−0.167	0.008

2.1 Structure formation simulations

We start by performing a very large dark matter only simulation of early structure formation, with $1624^3 \approx 4.3$ billion particles and

3248^3 grid cells[1] using the code PMFAST (Merz, Pen & Trac 2005). This allows reliable identification (with 100 particles or more per halo) of all haloes with masses $\sim 2 \times 10^9\,h^{-1}\,\mathrm{M}_\odot$ or larger. We compile and save the halo catalogues, in up to 100 time slices starting from high redshift ($z \sim 30$) to the observed end of reionization at $z \sim 6$. In what follows, we will refer to this simulation as high-resolution (HR) simulation. This HR simulation and in particular the halo catalogues based on it are used as the framework for our RT simulation which will be explained in detail in Section 2.2. In order to maximize the mass resolution, the dark matter particles are not labelled in the HR simulation, which does not allow us to identify the progenitors of any given structure at $z = 0$. We resolved this problem by resimulating the same initial conditions at lower resolution (called LR simulation hereafter) which allows for tagging of the particles. This enables us to identify the progenitors of haloes at $z = 0$ and to simultaneously follow their reionization and mass growth histories. To obtain the LR simulation, the original HR PMFAST initial conditions (with 1624^3 particles) were generated again using the same random seeds. They were then coarsened to 406^3 particles by averaging the properties (positions and velocity components) of every 4^3 neighbouring particles. We evolved these coarsened initial conditions from $z = 100$ to 0 using PKDGRAV, a fast parallel tree code written by Joachim Stadel and Tom Quinn (Stadel 2001).

2.2 The radiative transfer simulations

We proceed by applying our RT code to the HR simulation described above. Since RT simulations at the full grid size of our *N*-body simulations are still impractical, we follow the RT on coarser grids, of sizes 203^3. All identified haloes are assumed to be sources of ionizing radiation and each is assigned a photon emissivity proportional to its total mass, *M*, according to

$$\dot{N}_\gamma = f_\gamma \frac{M\Omega_\mathrm{b}}{\mu m_\mathrm{p} t_\mathrm{s} \Omega_0}, \tag{1}$$

where t_s is the source lifetime, m_p is the proton mass, μ is the mean molecular weight and f_γ is a photon-production efficiency which includes the number of photons produced per stellar atom, the star formation efficiency (i.e. what fraction of the baryons are converted into stars) and the escape fraction (i.e. how many of the produced ionizing photons escape the haloes and are available to ionize the IGM). Since we do include in the halo catalogue only haloes defined by more than 100 particles, this criterion introduces a minimum mass for haloes in order to act as ionizing sources. For our choice of the simulation parameters this corresponds to a mass threshold of $M_\mathrm{th} = 2.5 \times 10^9\,h^{-1}\,\mathrm{M}_\odot$ (*WMAP*1) and $2.2 \times 10^9\,h^{-1}\,\mathrm{M}_\odot$ (*WMAP*3). Note that this mass corresponds roughly to the halo mass above which a galaxy forming in it is largely unaffected by reionization (see Iliev et al. 2007, for discussion and references).

The RT is followed using our fast and accurate ray-tracing photoionization and non-equilibrium chemistry code C^2-RAY (Mellema et al. 2006a). The code has been tested in detail for correctness and accuracy against available analytical solutions and a number of other cosmological RT codes (Iliev et al. 2006a; Mellema et al. 2006a). The radiation is traced from every source on the grid to every cell using short characteristic ray tracing. The runs and notation are the same as the ones presented in Iliev et al. (2006b), Mellema et al. (2006b), Iliev et al. (2007). These include simulations with both *WMAP*1 and *WMAP*3 background cosmology. The runs for a given cosmology share the same underlying *N*-body simulation (but with different random realizations for *WMAP*1 and *WMAP*3), and each adopts different assumptions about the source efficiencies and the subgrid level of gas density fluctuations. In part of the simulations, a subgrid gas clumping is included, $C(z) = \langle n^2\rangle/\langle n\rangle^2$, which evolves with redshift according to

$$C_\mathrm{subgrid}(z) = 27.466\mathrm{e}^{-0.114z+0.001\,328\,z^2} \tag{2}$$

in *WMAP*1 cosmology and as

$$C_\mathrm{subgrid}(z) = 26.2917\mathrm{e}^{-0.1822z+0.003\,505\,z^2} \tag{3}$$

for *WMAP*3 cosmology. These fits were obtained from another set of two HR PMFAST *N*-body simulation, with box sizes $(3.5h^{-1}\,\mathrm{Mpc})^3$ and a computational mesh and number of particles of 3248^3 and 1624^3, respectively. The inclusion of gas clumping results in a slower propagation of the reionization fronts and a delay of the final overlap.

In what follows, we will concentrate on three cases, two 'extreme' models and an intermediate one. The extreme cases (in terms of z_ov, the redshift at which the final overlap is reached), are the following: *WMAP*1-f2000 (*WMAP*1, $f_\gamma = 2000$, no subgrid gas clumping) and *WMAP*3-f250C (*WMAP*3, $f_\gamma = 250$, with subgrid gas clumping). These two simulations should roughly bracket the allowed range in cosmological and reionization parameters. Among all of our RT simulations, the *WMAP*1-f2000 simulation has the earliest redshift of overlap, $z_\mathrm{ov} = 11.3$, while simulation *WMAP*3-f250C has the latest overlap, $z_\mathrm{ov} \sim 6.5$. We add a simulation in between those two cases: *WMAP*1-f250C (*WMAP*1, $f_\gamma = 250$, with subgrid gas clumping), resulting in $z_\mathrm{ov} = 8.2$. This allows us to study the effect of changing only the cosmology or changing only the reionizing photon-production efficiency. The lower efficiency of $f_\gamma = 250$ appears more realistic at present, and the corresponding cases match the late end of reionization at $z \sim 7$ well. We note that the delayed structure formation due to the lower power spectrum normalization, tilt and lower matter density in the favoured *WMAP*3 cosmology naturally predicts the lower integrated Thomson scattering optical depth the same measurements found, and thus do not seem to require a lower reionizing photon-production efficiency (Alvarez et al. 2006, but see also Haiman & Bryan 2006; Shull & Venkatesan 2007).

For the *WMAP*1 simulations, transmissive boundary conditions on the ray tracing were used. As a consequence, haloes close to the boundaries of our computational volume will be somewhat less affected by external radiation, particularly towards the end of reionization. Thus, in order to be conservative, we do not include in our analysis any haloes that are within $10h^{-1}$Mpc from the simulation boundary. The *WMAP*3 simulation utilized periodic boundary conditions, which allows for all haloes to be used in our analysis.

3 METHODS

3.1 Matching the HR and LR simulations

In order to investigate the reionization and formation history of a given halo, we first identify it at $z = 0$ in our LR simulation, using a spherical overdensity halo finder (see Macciò et al. 2007, for a detailed description). We then track the particles of the halo in consideration back to higher redshift in the LR simulation and match them to the HR simulation in order to analyse its formation and reionization history. This can only be done if the density distribution in the HR and LR simulation agree well; since two quite different

[1] $3248 = N_\mathrm{nodes}(512 - 2 \times 24)$, where $N_\mathrm{nodes} = 7$ (with four processors each), 512 cells is the Fourier transform size and 24 cells is the buffer zone needed for correct force matching on each side of the cube.

methods and resolutions are used for them, this merits checking and evaluating the closeness of the match between the two. If they match well, the location of the haloes which can be identified in the LR simulation should be similar to the location of the most massive haloes in the HR simulation (where the total number of identified haloes at any redshift is much higher than in the LR simulation). As a test, we identify for each halo in the LR simulation which is found by our spherical overdensity halo finder the nearest halo in the HR simulation which has a similar mass (within a factor of 2). At $z = 6$ in the *WMAP*3 simulation, we find that the median distance between the haloes in the two catalogues is 0.3 h^{-1} Mpc, with a similar result for the *WMAP*1 simulation. Since this distance is below the grid size of the RT code, we consider this reasonable agreement for our current purposes. However, for around 3 per cent of all cases, no nearby halo with similar mass is identified. This is not surprising given the fact that we use two different halo finders and have a large difference in resolution. Note that the median distance and the number of unmatched haloes decreases with increasing redshift. This reflects the fact that the DM distribution in the HR and LR simulation becomes more similar at high z, since the effects of different force resolution, etc., are diminished. As all of our comparisons between LR and HR simulations are done at times when the Universe is not yet completely reionized, i.e. $z > 6$, we consider the median distance and the fraction of unmatched haloes quoted above an upper limit.

In what follows, we will explain in more detail how the formation and the reionization history of a given $z = 0$ halo is investigated. We mark the particles that will end up in a given halo at $z = 0$ and track them back to simulation outputs at higher redshifts. At any redshift, we identify the centre of the halo progenitor as the densest particle (smoothing over the 32 closest neighbours) in the marked set and measure the fraction of reionized gas in the central cell and the 26 neighbouring cells, using the RT grid consisting of 203^3 cells. In this way, an offset of one RT cell (corresponding to $\sim 0.5\,h^{-1}$ Mpc) in each dimension is allowed between the centre of reionization in the HR simulation, and the location of the densest particle in the LR simulation. If the ionized fraction in any of those cells is higher than a threshold value of $x_{\rm th} = 0.7$, we define the halo as reionized and the corresponding reionization redshift $z_{\rm r}$ is set equal to the current output redshift. The particular value of $x_{\rm th}$ has a negligible impact on the final results thanks to the sharp transition across the ionization fronts (see Figs 1 and 2).

Next we check at which redshift the most massive progenitor of the halo in consideration first reaches a halo mass of $M_{\rm th}$ (as defined in Section 2.1), and define this as redshift of formation, $z_{\rm f}$. To do this, we again trace back the halo progenitor particles and identify the densest particle at each redshift. Again allowing for an offset of one cell, we consider a halo as formed if it is identified by our halo finder based on the HR simulation. Only for less than 2 per cent of all haloes, no formation redshift could be identified. They were removed from the sample.

Ionizing radiation in the ray-tracing simulation can, by definition, only be produced by haloes that have been identified; this allows us to clearly separate internally reionized haloes from externally reionized ones. If $z_{\rm r} > z_{\rm f}$ ($z_{\rm r} \leqslant z_{\rm f}$), the halo has been reionized externally (internally). For illustrative purposes, in Figs 1 and 2 we show the evolution of the ionization fronts around an internally and an externally reionized LG-like object, respectively.

Our method can occasionally fail if the halo progenitor under consideration has a very large extent (i.e. larger than two cells) and has two dense centres. If one of those is identified as the densest particle by our smoothing algorithm, while the other is recognized by the HR halo finder, external reionization will be always assumed. Eye inspection indicates that this happens in less than roughly 10 per cent of all cases we have identified as external reionization. On the other hand, if the reionization and the formation of a halo occur in between two time-steps, we always assume internal reionization. Although external reionization is also possible it is

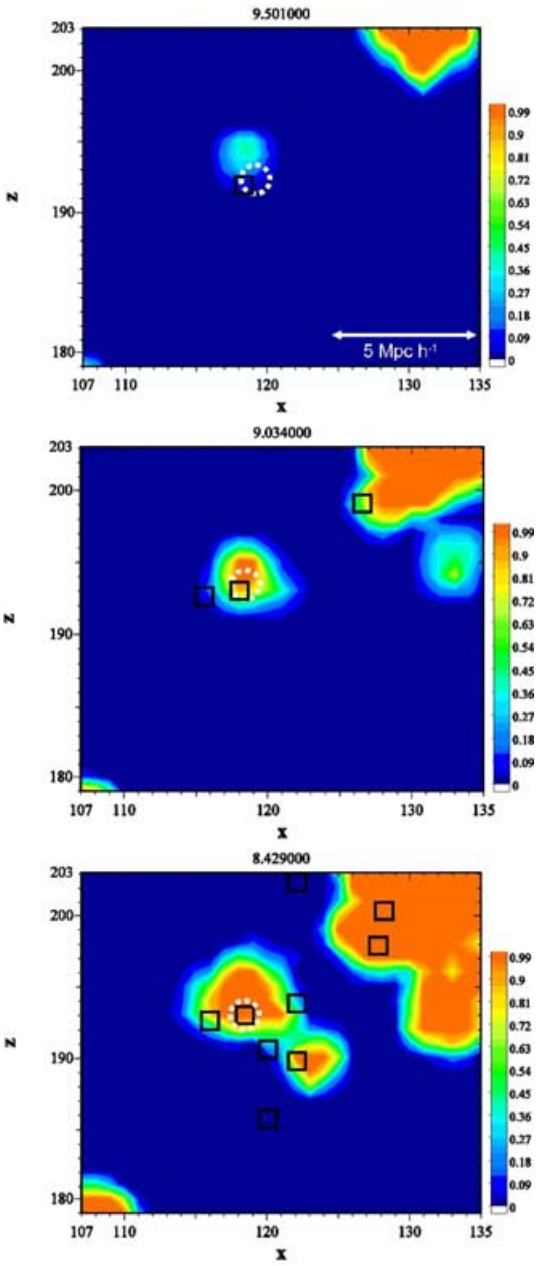

Figure 1. Reionization colour plot, showing an example of internal reionization. Redshifts are denoted on the top of the plots. The reionization status of the gas is shown in colours, dark blue showing completely neutral gas, orange showing the completely reionized gas. Black rectangles denote the position of identified haloes, the white dashed circle denotes the position of the LG progenitor, identified by its densest particles. The ionization state of the gas was identified in a slice with a thickness of one cell of the simulation outputs at different redshifts, with the position of the slice centred around the LG progenitor under consideration. Identified haloes are shown if they are within a box of volume 20^3 cells centred around the LG progenitor (i.e. can be up to 10 cells offset from the slice shown in the pictures).

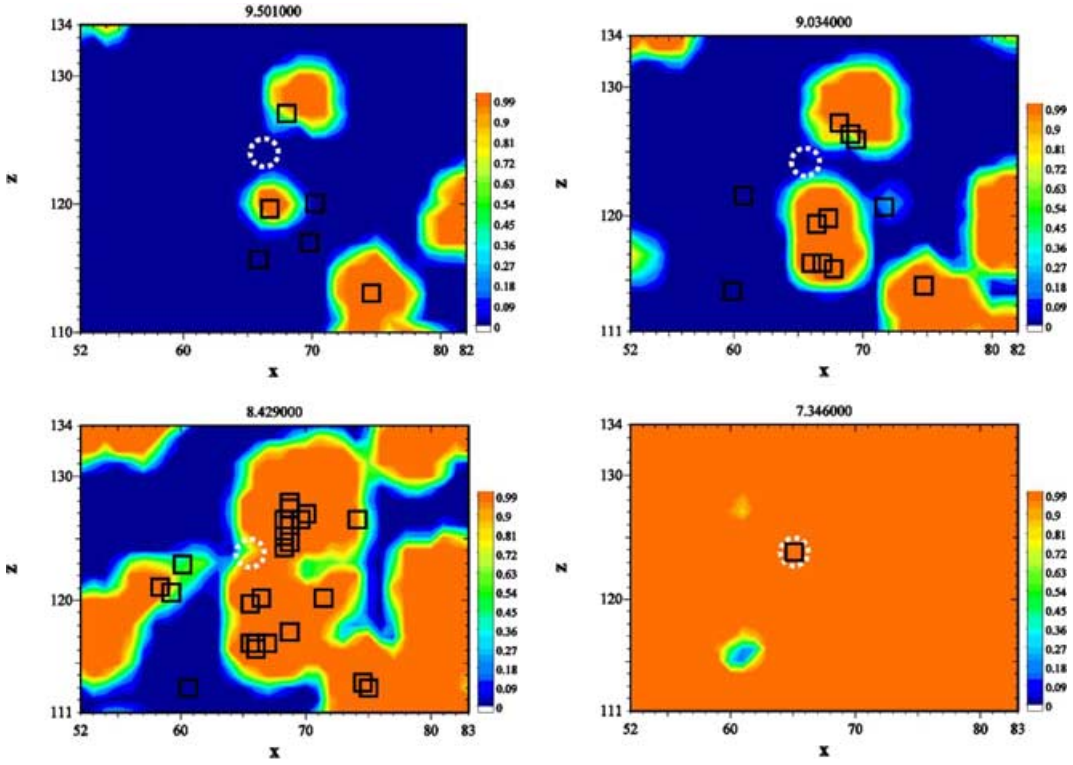

Figure 2. Reionization colour plot, showing an example of external reionization. Symbols/colours have the same meaning as in Fig. 1. At $z = 7.346$, the number of haloes is so large that we do not show them anymore in the plot.

unlikely. We did not find a way to solve these two issues, but we expect that their impact on our results should be modest, since these effects will both only occur for a small fraction of our haloes.

3.2 Sample selection

We have identified dark matter haloes at $z = 0$ in our LR simulation using our spherical overdensity halo finder. From this halo catalogue we selected three sets of objects for further consideration: (1) field haloes, (2) central objects of massive clusters, likely to correspond to central cD galaxies and (3) LG-like systems. As a subset of the field haloes, we also selected a sample of haloes likely to host an L* galaxy.

The sample sets of such systems were chosen as follows. The field halo samples consist of all the haloes with masses between 1.8×10^{11} and $3.7 \times 10^{13}\,h^{-1}\,\mathrm{M}_\odot$ that have been found by the spherical overdensity halo finder in both simulations. Such haloes are always isolated in the sense that they are not subhaloes in a larger group or cluster. In the *WMAP*1-f2000 and the *WMAP*1-f250C simulation, haloes with distances closer than $10\ h^{-1}$ Mpc from the edges of the simulation box were removed from the sample. In this way, we have identified 9683 haloes in the *WMAP*3-f250C simulation, and 7346 haloes in the *WMAP*1-f2000/*WMAP*1-f250C simulations. A sample of haloes likely to host an L* galaxy was chosen as follows. According to Madgwick et al. (2002), L* galaxies have a b_J luminosity of $1.1 \times 10^{10}\ h^{-1}\,\mathrm{L}_\odot$. A central or isolated L* galaxy is therefore most likely to be found in a halo with $\log(M) = 12.2$ ($h^{-1}\,\mathrm{M}_\odot$) in a *WMAP*3, and in a halo with mass $\log(M) = 12.3$ ($h^{-1}\,\mathrm{M}_\odot$) in a *WMAP*1 cosmology, following the relation between L_{cen} and halo mass in van den Bosch et al. (2007). The difference in the two cosmologies is mainly due to the different halo clustering properties. We select for our L* galaxy sample haloes with mass $\log(M) = 12.1$–$12.3 (h^{-1}\,\mathrm{M}_\odot)$ for the simulation based on *WMAP*3, and with $\log(M) = 12.2$–12.4 ($h^{-1}\,\mathrm{M}_\odot$) for the simulations based on *WMAP*1. We find 437 such haloes in the two simulations based on the *WMAP*1 cosmology, and 575 haloes in the *WMAP*3-f250C simulation.

The second set of haloes consists of the central objects in the 20 most massive galaxy clusters in each simulation. These massive objects are likely to correspond to central cluster cD galaxies. Finally, the third halo sample consists of all LG-like systems in our volume. These are identified as binary systems of dark matter haloes satisfying the following criteria (see Macciò, Governato & Horellou 2005, for details).

(i) The mass of each of the two haloes is between 4×10^{11} and $5 \times 10^{12}\,h^{-1}\,\mathrm{M}_\odot$.
(ii) The distance between the two haloes is below $700\,h^{-1}$ kpc.
(iii) The two haloes are moving towards each other.
(iv) There is no massive neighbour with a mass above 5×10^{11} closer than $2.1\,h^{-1}$ Mpc.

4 RESULTS

4.1 Reionization histories of galaxies of different mass and environment

On average, reionization *predates* formation for typical field haloes in all three simulation cases that we have considered. We compare the redshift of formation, z_{f}, the starting redshift of the halo reionization, z_{r}, and the redshift at which 70 per cent of the final halo mass is reionized, $z_{70\,\mathrm{per\,cent}}$, for all our halo samples (field haloes, haloes likely to host an L* galaxy, haloes likely to host a cD galaxy,

LG-like haloes) in Table 2. We note that by definition $z_r > z_{70\,\mathrm{percent}}$, and especially for massive haloes these redshifts could differ significantly since the material that will end up in the final halo is generally spread out over a very large region in space, and therefore a fairly long time could pass from start to finish of the reionization of that halo's material. As mentioned before, z_f is the redshift at which the largest progenitor of the halo reaches $M_{\rm th}$.

We find that external reionization occurs for roughly 80 per cent of all field haloes in the *WMAP*1-f2000 simulation, for 40 per cent in the *WMAP*1-f250C simulation and for ∼55 per cent in the *WMAP*3-f250C simulation. Apparently, our 'intermediate case' with a redshift of overlap in between the two other cases, has the lowest number of externally reionized haloes. This is caused by an interplay of two different effects. First, the higher the reionizing photon production, the more effective is a halo in reionizing its surroundings. If $f_\gamma = 2000$, each halo quickly reionizes a large volume, containing a mass ∼2000 times the halo mass, as recombinations are not very important. This explains the very high fraction of external reionization in the *WMAP*1-f2000 case, which indicates that in this case, few early collapsing haloes are responsible for most of the reionization of the matter in the universe. The influence of the cosmological framework is more complicated. As pointed out by Alvarez et al. (2006), structure formation is delayed by a factor of ∼1.4 in $(1 + z)$ in a *WMAP*3 cosmology compared to a *WMAP*1 cosmology. This means that structure formation becomes more extended in time in a *WMAP*3 cosmology, i.e. the time of formation of low- and high-mass haloes are further apart. In order for external reionization to occur, the radiation of an early collapsing halo has to reach other haloes before they have started to form. This window in time will be shorter in a *WMAP*1 cosmology than a *WMAP*3 cosmology, which explains the lower external fraction in the former case. This means that for a *WMAP*3 cosmology and a higher reionizing photon-production efficiency, the external fraction would be even above 80 per cent.

Another important outcome of our analysis is that differences in formation time cannot be directly translated into a difference in reionization time (cf. Table 2). Due to the contribution of external reionization, field galaxies 'catch up' with central cD galaxies when it comes to reionization. The time elapsed between formation and reionization (Δt) depends both on the cosmological model and on the reionization parameters. In the early reionization scenario *WMAP*1-f2000, Δt for field haloes and LG-like objects is always negative and maximal in absolute value, which means that these objects form a fairly long time after they have been reionized. Field haloes are reionized on average noticeably earlier in *WMAP*1-f2000 model than in the extended reionization scenarios. This is to be expected considering the much faster and earlier reionization in this case, allowing for significantly fewer field haloes to form before reionization. Some L* haloes in the *WMAP*1-f2000 simulation also do not manage to reach a mass of $M_{\rm th}$ before their reionization. Thus the coeval formation and reionization of L* haloes observed in the other two simulation cases is broken for early reionization. *WMAP*1-f250C and *WMAP*3-f250C share the same reionization parameterization. Thus, differences in Δt are due to the different cosmological models. The characteristic time-scale for structure formation is roughly the current Hubble time, $t_{\rm H}(z)$. So, in an attempt to scale out the cosmological dependence of Δt, we divided it by the Hubble time $t_{\rm H,\,50\,percent}$ when the ionized fraction (in mass) is 50 per cent to obtain $\Delta t^* = \Delta t / t_{\rm H,\,50\,per\,cent}$. Comparing the extended reionization scenarios, *WMAP*1-f250C and *WMAP*3-f250C, we see that Δt^* is very similar for all objects.

Haloes likely to host massive cD galaxies in centres of clusters are always internally reionized in all the different simulations. This

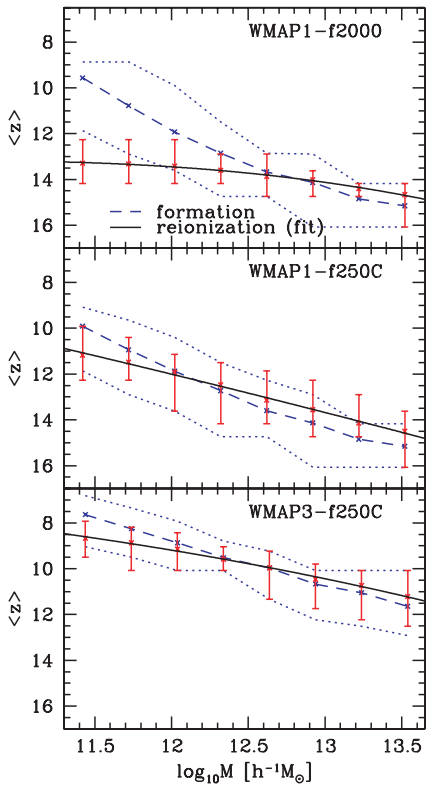

Figure 3. The average formation and reionization redshift (calculated converting redshift to look-back time and back) as a function of the halo mass for the *WMAP*1-f2000 (top panel), the *WMAP*1-f250C (middle panel) and the *WMAP*3-f250C (bottom panel) simulation. Error bars/dotted lines denote the 68 per cent confidence level. The black solid line is a fit to the average redshift of reionization, as explained in the text. Note that formation redshift here means the redshift at which $M > M_{\rm th}$.

reflects the strong inside-out nature of reionization. Reionization always starts from the highest density peaks, inside which cD haloes reside, and thus these are reionized early, regardless of the details of the reionization parameters and the background cosmology.

In summary, the timing of reionization compared to formation for L* and field haloes is sensitive to the reionization parameters (ionizing efficiency of the sources and gas clumping) and rather insensitive to the background cosmology, while in contrast the reionization history of central cD galaxies is largely independent of either the reionization parameters, or the cosmology.

In Fig. 3, we show the mean values of z_r and z_f as a function of the halo mass at $z = 0$. Averages are calculated by converting redshift to look-back time, averaging and converting the result again back to redshift. The reionization redshift as a function of halo mass at $z = 0$ can be fitted by a simple polynomial:

$$\langle z_r \rangle = ax + bx^2 + cx^3, \tag{4}$$

where $x = \log(M/\mathrm{M}_\odot)$, expressed without h^{-1}. We list the relevant values for a, b, c in Table 3.

There are clear trends for the redshift of formation and reionization as a function of halo mass. For lower mass haloes, reionization typically happens prior to their formation (external reionization), but for higher mass haloes, formation tends to predate reionization (internal reionization). As mentioned above, Alvarez et al. (2006) found that structure formation is delayed by a factor of 1.4 in $(1 + z)$ in a *WMAP*3 cosmology. We roughly find a similar change in the

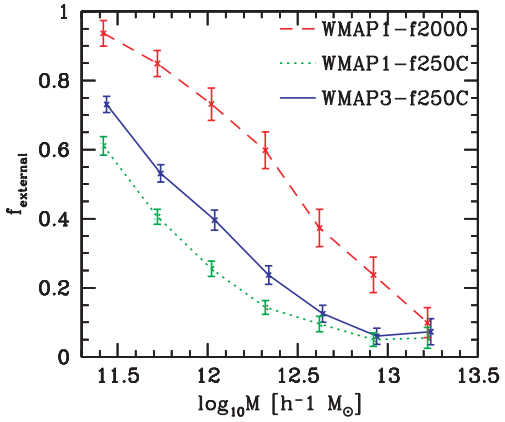

Figure 4. The fraction of externally ionized haloes as a function of halo mass respectively for the three simulations considered.

average formation time of a halo, comparing *WMAP*1 and *WMAP*3 cosmologies. The 68 per cent confidence level around average formation redshift is considerably larger for a *WMAP*1 cosmology than for a *WMAP*3 cosmology at low masses. However, this simply reflects the fact that a similar interval in time corresponds to a much larger interval in redshift at higher redshifts. Measured in look-back time, the scatter around the average formation redshift is very similar in the two cosmologies and even slightly higher for *WMAP*3 at low masses.

In Fig. 4, we show the fraction of externally reionized haloes as a function of halo mass. It is apparent that the probability of external reionization is strongly dependent on mass, mainly because the formation redshift and the mass of a halo are correlated, and haloes which form later have a higher probability of being externally reionized. We note that even if on average a halo forms after it vicinity has been reionized, the fraction of externally reionized haloes can still be rather low. The reason for this is that for many internally reionized haloes, the redshift of formation and the redshift of reionization are the same or at least very close. Thus, even a relatively small fraction of externally reionized haloes can shift the mean reionization redshift so that it predates the formation redshift.

Generally, one might expect that the probability of external reionization of a field galaxy could also depend upon the local overdensity around it, since the latter is closely related to the abundance of sources of ionizing radiation near the field galaxy in consideration. In Fig. 5 (upper panel) we plot the fraction of externally reionized field haloes as a function of the surrounding overdensity in collapsed haloes with mass $M > 5 \times 10^{12}\,h^{-1}\,\mathrm{M}_\odot$ at $z = 0$. The overdensity is measured within a sphere of radius $10\,h^{-1}$ Mpc centred on the halo in consideration, does not include this central halo, and is measured relative to the average density of the simulation box. Contrary to what one might expect, there is no clear trend.

This result persists if we change the mass limit on the surrounding collapsed haloes, or the radius of the sphere. In Fig. 5, bottom panel, we show for the example of the *WMAP*3-f250C simulation that the constant behaviour of the externally reionized halo fraction also persists if we divide the halo sample into different mass bins. As evident in Fig. 6, the reason for the constant behaviour of the external fraction with halo mass is that not only the reionization, but also the formation of a halo occurs at slightly lower redshifts in underdense regions, since the local 'clock' of structure formation is slower in voids. Therefore, we conclude that the environment of haloes does

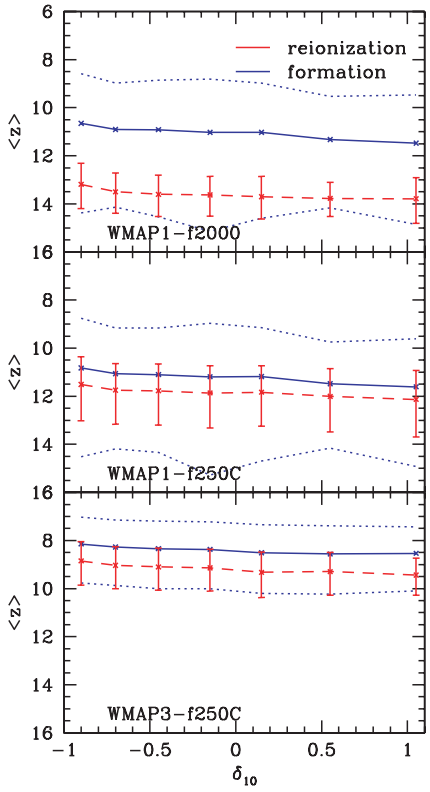

Figure 5. Top panel: The fraction of externally ionized haloes as a function of the overdensity by measuring only the mass in collapsed haloes with masses above 5×10^{12}. The overdensity is calculated with respect to the mean matter density in the simulation box. Results for all three simulations are shown. Error bars denote the 1σ error. Bottom panel: Same as shown top panel, for the *WMAP*3-f250C simulation only, but for three different bins regarding the mass of the halo in consideration. The way the surrounding overdensity is measured remains unchanged. For clarity, no error bars are shown.

not change the way in which they are reionized, at least if the dark matter halo is isolated. For cluster and group galaxies being part of a larger dark matter halo, this statement might not be correct anymore. Satellite galaxies in massive clusters that are close to the central cD galaxy will most probably be reionized by the time when 70 per cent of the dark matter mass surrounding the central cD galaxy itself is reionized. This is clearly earlier than the typical redshift where galaxies in the field are reionized. However, the difference is probably less dramatic than the difference in formation redshift. One could speculate that this means that galaxies in clusters are reionized internally more often than galaxies in the field. We have found this to be the case at least for the resolvable subhaloes in clusters, which we have identified with our subhalo finder SKID (Stadel 2001). However, since they are not a fair tracer of the subhalo population, we do not discuss our results in detail.

4.2 The reionization history of the Local Group

In this section, we study the reionization history of LG-like objects. As binary systems, LG-like objects might be expected to have a different average formation and reionization history than typical field galaxies. Our LG of galaxies also provides the most detailed set of observational data for testing the consequences of reionization on subsequent galaxy formation. We apply the same definitions of internal and external reionization we described above to our

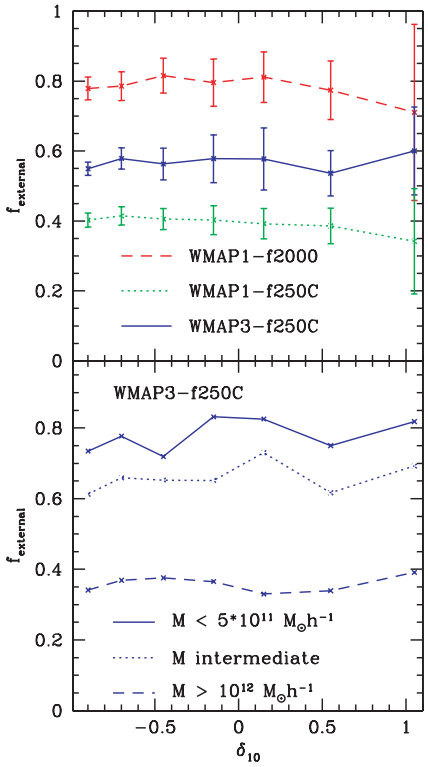

Figure 6. The average formation and reionization redshift (calculated converting redshift to look-back time and back) as a function of the overdensity measured only for the mass in collapsed haloes with masses above 5×10^{12}, for the *WMAP*1-f2000 (top panel), *WMAP*1-f250C (middle panel) and the *WMAP*3-f250C (bottom panel) simulation. Dotted lines/error bars denote the 1σ error.

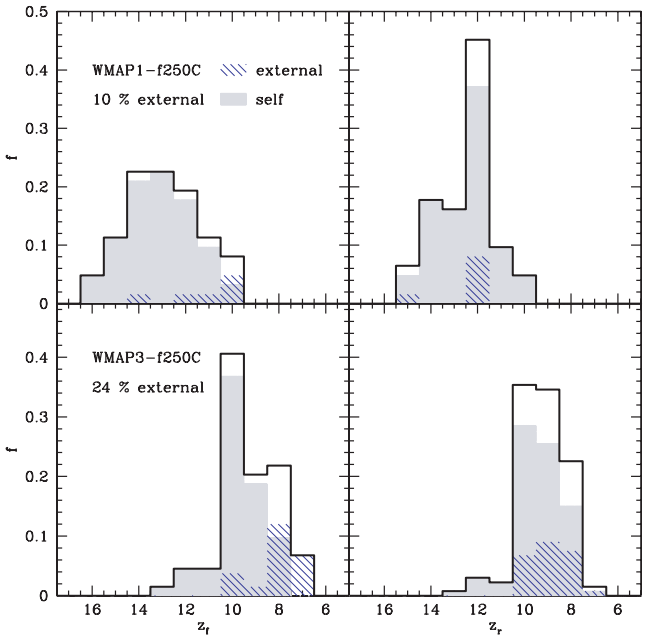

Figure 7. Comparison between formation redshift (z_f) and reionization redshift (z_r) for LGs that are externally (diagonal texture) and internally (grey area) reionized. Results are shown for the *WMAP*1-f250C and the *WMAP*3-f250C simulation. Again, z_f is defined as the redshift where the mass of the halo exceeds M_{th}.

LG-candidate sample. For *WMAP*3-f250C we find that 24 per cent (32 out of 133 LGs) are externally reionized. For *WMAP*1-f250C, the probability of external reionization is only ∼10 per cent (six out of 62 LG). As for L* and field galaxies, *WMAP*1-f2000 shows the highest fraction of external reionized LGs: 44 per cent (27 out of 62). In Fig. 7, we show the distribution of the reionization and formation redshifts of LG candidates for the two simulations with the lower reionization efficiency: *WMAP*1-f250C and *WMAP*3-f250C. As in Fig. 3 at the lower mass end, it is evident that the scatter in formation redshift is larger than the scatter in reionization redshift. This is caused by the contribution of external reionization.

To summarize, the probability for LG-like objects to be externally reionized is lower than the corresponding probability for low-mass field galaxies, which can be as high as 60–80 per cent. Compared to typical L* galaxies, LG-like systems form slightly earlier, get reionized slightly earlier and are somewhat less likely to be externally reionized than L* galaxies.

5 POTENTIAL CAVEATS

All of our simulations resolve only haloes with masses above $M_{th} \sim 2 \times 10^9\,M_\odot$ and these are the only sources which contribute to the reionization of the universe in this set of simulations. However, in hierarchical structure formation scenarios the smallest haloes form first and merge up. Thus it is expected that the first sites of star formation were 'minihaloes' with a mass roughly between 10^4 and $10^8\,h^{-1}\,M_\odot$. By definition the minihaloes have virial temperatures below 10^4 K, where the radiative gas cooling through hydrogen and helium atomic lines is not efficient. Thus, these haloes have to rely on the much less efficient molecular line cooling for their star formation. However, the hydrogen molecules are easily destroyed by radiative feedback (e.g. Haiman, Abel & Rees 2000) and thus it is generally expected that most minihaloes were 'sterilized' and in most cases did not form stars (e.g. Shapiro et al. 2004; Iliev et al. 2005, and references therein). On the other hand, haloes with a mass between 10^8 and $10^9\,M_\odot$, which are also not resolved in our simulations, are able to cool efficiently and may actually be an important source of ionizing radiation. Iliev et al. (2007) have performed a number of smaller scale HR simulations of reionization, with a simulation volume $(35\,h^{-1}\,\mathrm{Mpc})^3$, which include radiation from these smaller haloes. The most important effect is that reionization starts much earlier than without those sources. However, due to Jeans mass filtering in the ionized regions and the strong clustering of haloes around the density peaks, the majority of these low-mass haloes are suppressed throughout most of the reionization processes and hence their effect is mostly limited to the early stages of reionization and the progress of reionization is delayed. The time of overlap and the large-scale geometry of reionization are both largely dominated by the high-mass haloes and thus are not strongly affected by the absence of low-mass haloes in the simulations.

Could the inclusion of low-mass haloes and minihaloes significantly modify our results? A halo with a mass of $10^8\,M_\odot$ can reionize a mass between 2.5×10^{10} and $2.5 \times 10^{11}\,M_\odot$ (somewhat decreased once recombinations are accounted for) during its lifetime of ∼20 Myr (before star formation shuts off again due to feedback, and recombinations set in, decreasing the reionized fraction further). Thus, in order to reionize a (proto)halo with a mass around $10^{12}\,M_\odot$, several $10^8\,M_\odot$ haloes ought to have formed at very similar times within the region considered. They should also have been spaced far enough apart so that the halo forming first

does not suppress star formation in the other haloes. Even if this were the case, this group of $\sim 10^8\,M_\odot$ haloes would most probably quickly merge, forming a halo with a mass above $10^9\,M_\odot$, which would be resolved in our simulations. Moreover, regions which contain only 10^8–$10^9\,M_\odot$ haloes, but not any of the more massive ones tend to be near the boundaries of the ionized regions, and are thus quickly overrun by the expanding I-fronts. Furthermore, both low-mass atomically cooling haloes and minihaloes are strongly clustered around the density peaks, which are the first regions to be reionized, as we have shown. Therefore the vast majority of these small haloes would be affected by Jeans mass filtering. As a consequence, haloes forming after their vicinity is ionized would not be able to accrete gas, while haloes that have formed before their region became ionized would either not accrete more gas and thus have their star formation shut off (in the case of low-mass sources), or would be photoevaporated (in the case of minihaloes).

For all these reasons, we expect that neither haloes with masses between 10^8–$10^9\,M_\odot$, nor minihaloes would change our average reionization redshifts significantly and hence would not modify our results for the external/internal reionization fractions. Once future cosmological simulations become large enough to allow resolving low-mass haloes in a large volume, it would be interesting to verify if our assertions here are correct and evaluate the level of this effect precisely.

Furthermore, the reionization parameters, photon-production efficiencies and small-scale gas clumping (and to lesser level, also the background cosmology) are still quite uncertain. We have addressed this by comparing three reionization scenarios which roughly bracket the expected range of reionization histories, from the very early reionization given by f2000_*WMAP*1 (high-efficiency sources, no subgrid clumping, *WMAP*1 cosmology), to the late overlap, extended reionization scenarios, f250C_*WMAP*1 and f250C_*WMAP*3 (low-efficiency sources, subgrid clumping, *WMAP*1 or *WMAP*3 cosmology). Most of the reasonable reionization scenarios which satisfy the current observational constraints should fall between these cases. Further improvement would require better, more detailed observational data which would constrain the reionization scenarios (and thus the reionization parameters) better.

6 IMPLICATIONS OF EXTERNAL VERSUS INTERNAL REIONIZATION REGARDING GALAXY PROPERTIES

Reionization can affect the properties of galaxies in many ways, and the relative timing of reionization across the mass scales will leave distinct observable signatures.

(i) The mode of galaxy formation may be fundamentally different between haloes less massive and more massive than $10^{12}\,M_\odot$. Late-forming haloes that are externally ionized will have hotter, more extended and smoother gas distributions. The gas accretion into the galaxy will proceed differently, perhaps providing an explanation for the red–blue galaxy sequence, bulgeless discs, lower baryon fractions in less massive galaxies, etc.

(ii) Early star formation will be affected, since stars forming in ionized gas may have different properties than stars forming in neutral gas. According to Johnson & Bromm (2006), Population II.5 (Pop II.5) could have formed from primordial gas that is strongly ionized since the free-electron-catalysed formation of molecules enables enhanced gas cooling. Similarly, Nagakura & Omukai (2005) predict the formation of low-mass stars in ionized gas with very low metallicity. External reionization provides an alternative pathway to Pop II.5 star formation.

(iii) The abundance of Galactic satellites has been reconciled with observational data using the idea that reionization suppresses the formation of late-forming haloes – only the rare peaks that collapse before reionization can cool gas to form stars. If the gas in a late-forming galaxy is externally reionized it may suppress the formation of some or even all of its satellite population.

(iv) The radial distribution of old stars in the Galactic halo might reflect the rarity of the density peaks in which they formed at the epoch of reionization (Diemand, Madau & Moore 2005; Moore et al. 2006). If stars form only in the rarest peaks, then their final distribution can be highly concentrated with a radial profile as steep as r^{-4}. Thus, externally reionized galaxies may be expected to have steeper diffuse stellar halo profiles.

(v) Similar to the old stellar halo, globular cluster formation may be truncated at reionization, altering the relative abundances and radial distributions of the old blue population in galaxies of different masses and environments. Rhode et al. (2005) found that the number of old blue galactic clusters (GCs) per galaxy stellar mass increases with increasing mass for cluster ellipticals, while it seems to be constant for spiral galaxies in the field. They suggest that the reason for this is that more massive elliptical galaxies assemble earlier and have more time to form blue GC before reionization, assuming that reionization happens at a fixed point in time. Although we find that reionization will occur considerably earlier in massive elliptical galaxies than for low-mass field galaxies, their redshift of formation is shifted even more strongly, as they are usually internally reionized. Thus it is indeed the case that typically more time elapses between the formation and reionization of massive cluster ellipticals than for field galaxies.

We conclude that it may already be possible to discriminate between galaxies that have been reionized internally or externally using one or more of the above characteristics. This will be an interesting new and complementary way to probe the history of reionization in the Universe and its effect on galaxy formation.

7 SUMMARY AND DISCUSSION

The reionization history of a given galaxy is strongly dependent on its mass due to the correlation between galaxy mass and formation redshift. Higher mass haloes on average form earlier and are also reionized earlier. The lower the mass of a halo, the more important does external reionization (i.e. reionization emanating from sources outside the halo) become. The effect of the large-scale environment on the reionization history, on the other hand, is negligible for field haloes. By using a simple polynomial fit, we can parametrize the average reionization redshift of a galaxy as a function of halo mass for three different combinations of cosmology and reionizing photon-production efficiency. Typical L^* galaxies and LG-like systems are reaching reionization considerably before the final overlap, at a redshift where roughly half of the Universe is reionized. Very massive, elliptical galaxies in clusters are reionized even earlier and are always internally reionized. Our prescription for the reionization redshift as a function of galaxy mass might be of use for semi-analytical models of galaxy formation. Normally, these models assume a fixed, fairly low redshift of reionization of around $z \sim 7$ (e.g. Croton et al. 2006), from which the baryon fraction in a low-mass haloes can be calculated, given redshift and halo mass (Gnedin 2000; Kravtsov et al. 2004). Using our fitting formulae, one could utilize a more realistic reionization redshifts in semi-analytical models by introducing

a dependence on the mass of the halo in which a given subhalo ends up. This may help alleviate the problem of the overproduction of satellite galaxies in massive clusters in semi-analytical models (Weinmann et al. 2006).

We suggest that whether a galaxy experiences internal or external reionization might affect its properties considerably. Externally reionized haloes could experience different gas accretion; could have a different first generation of stars (i.e. Pop II.5 instead of Pop III); may host a lower number of satellite galaxies and blue globular clusters; and could have steeper diffuse stellar halo profiles.

ACKNOWLEDGMENTS

Part of the *N*-body simulations have been performed on the zBox2 supercomputer at the University of Zurich (http://www-theorie.physik.unizh.ch/~dpotter/zbox2/). We thank D. Potter and J. Stadel for building and maintaining the zBox2. We also thank F. van den Bosch and M. Volonteri for useful discussion and an anonymous referee for comments which helped us improve the paper. SMW has been partially supported by the Swiss National Science Foundation (SNF).

REFERENCES

Alvarez M. A., Shapiro P. R., Ahn K., Iliev I. T., 2006, ApJ, 644, L101
Barkana R., Loeb A., 2004, ApJ, 609, 474
Bullock J. S., Kravtsov A. V., Weinberg D. H., 2000, ApJ, 539, 517
Croton D. J. et al., 2006, MNRAS, 365, 11
Dekel A., Silk J., 1986, ApJ, 303, 39
Diemand J., Madau P., Moore B., 2005, MNRAS, 364, 367
Dijkstra M., Haiman Z., Rees M. J., Weinberg D. H., 2004, ApJ, 601, 666
Efstathiou G., 1992, MNRAS, 256, 43P
Gnedin N. Y., 2000, ApJ, 542, 535
Haiman Z., Bryan G. L., 2006, ApJ, 650, 7
Haiman Z., Abel T., Rees M. J., 2000, ApJ, 534, 11
Iliev I. T., Shapiro P. R., Raga A. C., 2005, MNRAS, 361, 405
Iliev I. T. et al., 2006a, MNRAS, 371, 1057
Iliev I. T., Mellema G., Pen U.-L., Merz H., Shapiro P. R., Alvarez M. A., 2006b, MNRAS, 369, 1625
Iliev I. T., Mellema G., Shapiro P. R., Pen U. L., 2007, MNRAS, 376, 534
Johnson J. L., Bromm V., 2006, MNRAS, 366, 247
Klypin A., Kravtsov A. V., Valenzuela O., Prada F., 1999, ApJ, 522, 82
Kravtsov A. V., Gnedin O. Y., Klypin A. A., 2004, ApJ, 609, 482
Macciò A. V., Governato F., Horellou C., 2005, MNRAS, 359, 941
Macciò A. V., Dutton A. A., van den Bosch F. C., Moore B., Potter D., Stadel J., 2007, MNRAS, 378, 55
Madgwick D. S. et al., 2002, MNRAS, 333, 133
Mellema G., Iliev I. T., Alvarez M. A., Shapiro P. R., 2006a, New Astron., 11, 374
Mellema G., Iliev I. T., Pen U.-L., Shapiro P. R., 2006b, MNRAS, 372, 679
Merz H., Pen U.-L., Trac H., 2005, New Astron., 10, 393
Moore B., Ghigna S., Governato F., Lake G., Quinn T., Stadel J., Tozzi P., 1999, ApJ, 524, L19
Moore B., Diemand J., Madau P., Zemp M., Stadel J., 2006, MNRAS, 368, 563
Nagakura T., Omukai K., 2005, MNRAS, 364, 1378
Navarro J. F., Steinmetz M., 1997, ApJ, 478, 13
Rhode K. L., Zepf S. E., Santos M. R., 2005, ApJ, 630, L21
Santos M. R., 2003, in Kissler-Patig M., ed., Proc. ESO Workshop, Extragalactic Globular Cluster Systems. Springer Verlag, Berlin, p. 348
Shapiro P. R., Iliev I. T., Raga A. C., 2004, MNRAS, 348, 753
Shull M., Venkatesan A., 2007, preprint (astro-ph/0702323)
Spergel D. N. et al., 2003, ApJS, 148, 175 (*WMAP*1)
Spergel D. N. et al., 2007, ApJS, 170, 377 (*WMAP*3)
Stadel J. G., 2001, PhD thesis, Univ. Washington
Thoul A. A., Weinberg D. H., 1996, ApJ, 465, 608
Tully R. B., Somerville R. S., Trentham N., Verheijen M. A. W., 2002, ApJ, 569, 573
van den Bosch F. C. et al., 2007, MNRAS, 376, 841
Weinmann S. M., van den Bosch F. C., Yang X., Mo H. J., Croton D. J., Moore B., 2006, MNRAS, 372, 1161

This paper has been typeset from a TEX/LATEX file prepared by the author.